Survey of the ^{8}He properties within a microscopic multiphonon approach

G. De Gregorio,[1,2] F. Knapp,[3] P. Veselý,[4] and N. Lo Iudice[5]

[1]*Dipartimento di Matematica e Fisica, Università degli Studi della Campania "Luigi Vanvitelli," viale Abramo Lincoln 5, I-81100 Caserta, Italy*

[2]*Istituto Nazionale di Fisica Nucleare, Complesso Universitario di Monte S. Angelo, Via Cintia, I-80126 Napoli, Italy*

[3]*Institute of Particle and Nuclear Physics, Faculty of Mathematics and Physics, Charles University, V Holešovičkách 2, 180 00 Prague, Czech Republic*

[4]*Nuclear Physics Institute, Czech Academy of Sciences, 250 68 Řež, Czech Republic*

[5]*Dipartimento di Fisica, Università di Napoli Federico II, 80126 Napoli, Italy*

(Received 5 May 2023; revised 6 July 2023; accepted 2 August 2023; published 21 August 2023)

Bulk properties, spectrum, and nuclear response of ^{8}He are investigated within the equation of motion phonon method, which generates an orthonormal basis of n-phonon states ($n = 0, 1, 2, 3 \ldots$) whose constituents are Tamm-Dancoff phonons. The basis is free of any contamination induced by the center-of-mass motion, in virtue of a procedure exploiting the singular value decomposition of rectangular matrices. A self-consistent calculation is performed within a space spanned by a basis of n-phonon states up to $n = 3$ using a potential derived from the chiral effective field theory. The Hartree-Fock single-particle states are obtained from a harmonic-oscillator space including all major shells up to $N_{\max} = 12$. The calculation is exact up to $n = 2$, whereas the three-phonon ($n = 3$) states are assumed to be composed of noninteracting $n = 1$ and $n = 2$ constituent phonons. It yields bulk and spectroscopic observables consistent with the available experimental data and provides an electric dipole response exhibiting distinctive signatures.

DOI: 10.1103/PhysRevC.108.024316

I. INTRODUCTION

Detecting the nuclei far from stability and exploring their properties represents a fascinating challenge for nuclear experimentalists and theorists. While a great effort is being made for creating new or upgrading existing radioactive beam facilities [1], the past experiments have produced already several radioactive isotopes exhibiting distinctive features.

The very light neutron-rich ^{6}He and ^{8}He isotopes characterized by small separation energies and large radii [2,3] represent a paradigmatic example. The properties of ^{6}He qualify this exotic isotope as a Borromean system [4], whereas ^{8}He is a halo nucleus having the largest neutron to proton ratio with a skin of the four valence neutrons around a tightly bound ^{4}He core.

Several theoretical *ab initio* investigations have been devoted to these two isotopes. Among them, a coupled-cluster (CC) calculation using a Berggren single-particle (s.p.) basis [5], a hyperspherical harmonics approach [6,7], no-core shell model (NCSM) calculations using a harmonic-oscillator (HO) [8–10] or a Coulomb-Sturmian s.p. basis [11]. Closely related is a calculation in a restricted SM space using an effective interaction derived from chiral potentials through a CC similarity transformation [12].

Important contributions have come from approaches of different nature. Among them, a quantum Monte Carlo calculation using a realistic NN + 3N potential [13], a phenomenological Gamow (G)SM approach [14,15], a cluster orbital SM applied to a five-body system composed of four neutrons plus ^{4}He [16,17], and an analysis of scattering data using a sum of Gaussians for determining the neutron versus proton density distributions [18].

In this paper, we will focus on ^{8}He. Its bulk properties have been determined with high precision. With respect to ^{6}He, it has a larger neutron separation energy [19] and a smaller charge radius [20,21], suggesting a $0p_{3/2}$ subshell closure. It has also a slightly larger matter radius [2,22]. There are only unbound excited levels. They have been searched through transfer [23] and breakup [24] reactions as well as via Coulomb excitations [25,26]. These experiments did not converge to an unanimous unambiguous conclusion about the energy and nature of the lowest resonant state. It was not clear whether one is dealing with a soft dipole resonance or a 2^+ level. This uncertainty has been seemingly solved by an analysis of the data produced by a recent low-energy inelastic proton-scattering experiment, which ruled out the dipole nature of the resonance and lead to the conclusion that the first excited state is an unbound 2^+ at 3.54(6) MeV [27]. A high statistic experiment planned at RIKEN devoted to the determination of the dipole strength should hopefully shed more light on the subject (see Ref. [28] for reference).

This ongoing experiment has stimulated new theoretical investigations, an *ab initio* CC study [28], a random-phase approximation (RPA) calculation framed within the energy density functional (EDF) context [29], and a cluster shell model analysis [30].

Here, we investigate thoroughly this nucleus within the equation of motion phonon method (EMPM) [31,32]. In its updated formulation [33], the method constructs and solves iteratively a set of equations of motion, which yields states composed of an arbitrary number ($n = 2, 3, \ldots$) of particle-hole (p-h) or two-quasiparticle [34] Tamm-Dancoff (TD) phonons. These states, added to the unperturbed ground ($n = 0$) and TD ($n = 1$) states, form a n-phonon ($n = 0, 1, 2, 3 \ldots$) orthonormal basis which is adopted to solve the full eigenvalue problem under no approximations apart from those induced by the finite dimensions of the s.p. and multiphonon spaces.

The method is free of any spurious contamination coming from the center-of-mass (c.m.) motion under no constraints and for any s.p. basis. This is achieved in two steps. We first decouple the c.m. from the TD states [35] by exploiting the Gram-Schmidt orthogonalization method. We then remove the residual contaminations from the multiphonon basis states by resorting to the singular value decomposition (SVD) of rectangular matrices [36]. In such a c.m. free formulation, the method could be applied with a fair success to the study of bulk and spectroscopic properties of ^{4}He [37]. The advantage of adopting the c.m. free EMPM with respect to the extensions of RPA and TDA was illustrated through numerical applications in Ref. [38].

In the present paper, we have used the NNLO$_{\rm sat}$ chiral potential [39], to be referred to as V_S, to generate a Hartee-Fock (HF) basis in a HO space including 13 major shells ($N_{\rm max} = 12$) and, then, solved the eigenvalue problem in a space spanned by the n-phonon basis up to $n = 3$. The calculation is exact up to $n = 2$ whereas the three-phonons are treated in the diagonal approximation, which consists in neglecting the interaction between the constituent $n = 1$ and $n = 2$ phonons.

II. BRIEF OUTLINE OF THE METHOD

Assuming known the $(n-1)$-phonon basis states $|\alpha_{n-1}\rangle$ of energies $E_{\alpha_{n-1}}$, we construct the set of redundant states

$$|\lambda\alpha_{n-1}\rangle = O^\dagger_\lambda |\alpha_{n-1}\rangle , \tag{1}$$

where

$$O^\dagger_\lambda = \sum_{ph} c^\lambda_{ph} a^\dagger_p b_h \tag{2}$$

creates a TD phonon of energy E_λ out of HF vacuum $|0\rangle$ through the action of the particle ($a^\dagger_p = a^\dagger_{x_p j_p m_p}$) and hole ($b_h = (-)^{j_h+m_h} a_{x_h j_h -m_h}$) creation operators.

We first extract from the redundant set a basis of linearly independent (but not orthogonal) states $|\lambda\alpha_{n-1}\rangle$ through the Cholesky decomposition method and use this basis to derive and solve the eigenvalue problem within the n subspace. To this purpose, we start with the equations of motion

$$\langle\alpha_{n-1}| [O_\lambda, H] |\alpha_n\rangle = (E_{\alpha_n} - E_{\alpha_{n-1}}) \langle\lambda\alpha_{n-1} |\alpha_n\rangle . \tag{3}$$

After expanding the commutator and performing other additional manipulations, we get the generalized eigenvalue equations

$$(\mathcal{H} - E)DC = 0, \tag{4}$$

or, more explicitly,

$$\sum_{jk} \left(\mathcal{H}^{\alpha_n}_{ik} - E_{\alpha_n}\delta_{ik}\right)\mathcal{D}^{\alpha_n}_{kj} C^{\alpha_n}_j = 0. \tag{5}$$

Here,

$$\begin{aligned}\mathcal{H}^{\alpha_n}_{ik} &= \mathcal{H}^{\alpha_n}_{(\lambda\alpha_{n-1})(\lambda'\alpha'_{n-1})} \\ &= (E_\lambda + E_{\alpha_{n-1}})\delta_{\lambda\lambda'}\delta_{\alpha_{n-1}\alpha'_{n-1}} + \mathcal{V}^{\alpha_n}_{(\lambda\alpha_{n-1})(\lambda'\alpha'_{n-1})},\end{aligned} \tag{6}$$

where $\mathcal{V}^{\alpha_n}_{(\lambda\alpha_{n-1})(\lambda'\alpha'_{n-1})}$ defines the phonon-phonon interaction, and

$$\mathcal{D}^{\alpha_n}_{kj} = \mathcal{D}^{\alpha_n}_{(\lambda\alpha_{n-1})(\lambda'\alpha'_{n-1})} = \langle\lambda'\alpha'_{n-1} |\lambda\alpha_{n-1}\rangle \tag{7}$$

is the overlap or metric matrix which preserves the Pauli principle. The expressions of $\mathcal{D}$ and $\mathcal{V}$ can be found, for instance, in Ref. [33].

At this stage, we exploit the SVD method [36] to single out and remove the spurious states. The resulting transformed intrinsic states satisfy the transformed eigenvalue equation

$$(\mathcal{H}' - E)D'C' = 0. \tag{8}$$

The c.m. free n-phonon eigenstates so obtained can be recast in terms of the original basis

$$|\alpha_n\rangle = \sum_{\lambda\alpha_{n-1}} C^{\alpha_n}_{\lambda\alpha_{n-1}} |\lambda\alpha_{n-1}\rangle . \tag{9}$$

The iteration of the procedure up to an arbitrary n produces a set of states which, added to the HF vacuum ($|0\rangle$) and the TD phonons ($\{|\alpha_1\rangle\} = \{|\lambda\rangle\}$), form an orthonormal basis $\{|\alpha_n\rangle\}$ ($n = 0, 1, 2, 3 \ldots$).

Such a basis is used for constructing and solving the eigenvalue problem in the full space

$$\sum_{\alpha_n\beta_{n'}} [(E_{\alpha_n} - \mathcal{E}_\nu)\delta_{\alpha_n\beta_{n'}} + \mathcal{V}_{\alpha_n\beta_{n'}}]\mathcal{C}^\nu_{\beta_{n'}} = 0, \tag{10}$$

where $\mathcal{V}_{\alpha_n\beta_{n'}} = 0$ for $n' = n$.

The coupling of the n-phonon $|\alpha\rangle = |\alpha_n\rangle$ to the n'-phonon states $|\beta'\rangle = |\beta_{n'}\rangle$ has the structure

$$\mathcal{V}_{\alpha\beta'} = \sum_{\lambda'\alpha'} \mathcal{V}^{\lambda'}_{\alpha\alpha'} \langle\lambda'\alpha' |\beta'\rangle \tag{11}$$

for $n' = n + 1$ and

$$\mathcal{V}_{\alpha\beta'} = \sum_{\alpha_2} \langle 0| H |\alpha_2\rangle \langle\alpha_2\alpha |\beta'\rangle \tag{12}$$

for $n' = n + 2$. The formulas giving $\mathcal{V}^{\lambda'}_{\alpha\alpha'}$ and $\langle 0| H |\alpha_2\rangle$ can be found elsewhere [37]. The solution of the final eigenvalue Eq. (10) yields the eigenvectors ($n = 0, 1, 2, 3 \cdots$)

$$|\Psi_\nu\rangle = \sum_{n,\alpha_n} \mathcal{C}^\nu_{\alpha_n} |\alpha_n\rangle . \tag{13}$$

III. NUMERICAL IMPLEMENTATION AND RESULTS

We adopt a Hamiltonian of the form

$$H = T_{\rm int} + V, \tag{14}$$

where $T_{\rm int}$ is the intrinsic kinetic energy and V is V_S [39], obtained by optimizing simultaneously the two-body and three-body components of the χEFT potential at N2LO. The full three-body force, limited to an energy cutoff $E_{3\,\rm max} = 12\hbar\omega$, is used to generate the HF basis. It is, instead, truncated at the normal ordered two-body level in solving the multiphonon eigenvalue problem. This approximation was discussed in CC using $V_{\rm low\kappa}$ plus a 3N force [40]. More recent investigations were carried within CC and NCSM using chiral NN + 3N Hamiltonians evolved through the similarity renormalization group [41], and in a CC approach to nucleonic matter using the $V_{\rm opt}$ potential plus a 3N force derived from the chiral effective field theory at N2LO [42].

The numerical procedure goes through the following steps: (i) Derive a HF basis from a HO space of dimensions $N_{\rm max}$ and frequency ω.; (ii) use the HF states to create the TD phonon basis; (iii) generate the n-phonon ($n = 2, 3\ldots$) basis by deriving and solving iteratively the EMPM Eq. (8); (iv) the basis so constructed is adopted to solve the final eigenvalue problem in the multiphonon space [Eq. (10)]. We will examine the ground-state properties, the spectrum, and the $E1$ response.

The HF basis was generated from a HO space of frequency ω and including all major shells up to $N_{\rm max}$. The eigenvalue Eq. (8) were solved exactly up to two phonons ($n = 2$). The three phonons were treated in the diagonal approximation, which consists in neglecting the phonon-phonon interaction $\mathcal{V}_{\lambda\alpha\lambda'\alpha'}$ in Eq. (6). All the states of energies $E_{\beta_3} \simeq E_{\alpha_2} + E_\lambda <$ 180 MeV were included. We have kept only the leading-order term of the overlap matrix [Eq. (7)] in computing the matrix elements $\mathcal{V}_{\alpha_1\beta_3}$ [Eq. (12)] and $\mathcal{V}_{\alpha_2\beta_3}$ [Eq. (11)], which couple the three-phonon $|\beta_3\rangle$ to the one-phonon $|\alpha_1 = \lambda\rangle$ and two-phonon $|\alpha_2\rangle$ states, respectively. Given the huge dimensions of the Hamiltonian matrix, we have extracted only the eigenstates of excitation energies $\omega_\nu = \mathcal{E}_\nu - \mathcal{E}_0 \leqslant 60$ MeV for $J^\pi = 1^-$ and $\omega_\nu \leqslant 20$ MeV for the other J^π.

A. Ground state

We have studied the convergence of the ground state energy versus the HO dimensions $N_{\rm max}$ and frequency by performing an exact calculation within the multiphonon space encompassing up to the full two-phonon basis. As shown in Fig. 1(a) the convergence is reached at $N_{\rm max} \approx 10$ and $\hbar\omega \approx 20$ MeV. For our spectroscopic studies we have used $N_{\rm max} = 12$ and $\hbar\omega = 16$ MeV, which is short from reaching convergence and came out to be the optimal frequency within the more complete CC calculation [28]. This implies an uncertainty of $\approx$1 MeV, which comes mainly from the spreading with respect to $\hbar\omega$. The inclusion of the three phonons adds only $\sim$200 keV. Thus, the final energy is $\mathcal{E}_0 = -25(1)$ MeV, still fairly distant from the experimental value $E^{\rm exp} = -31.3961$ MeV and from theoretical estimates using the same potential [28,39].

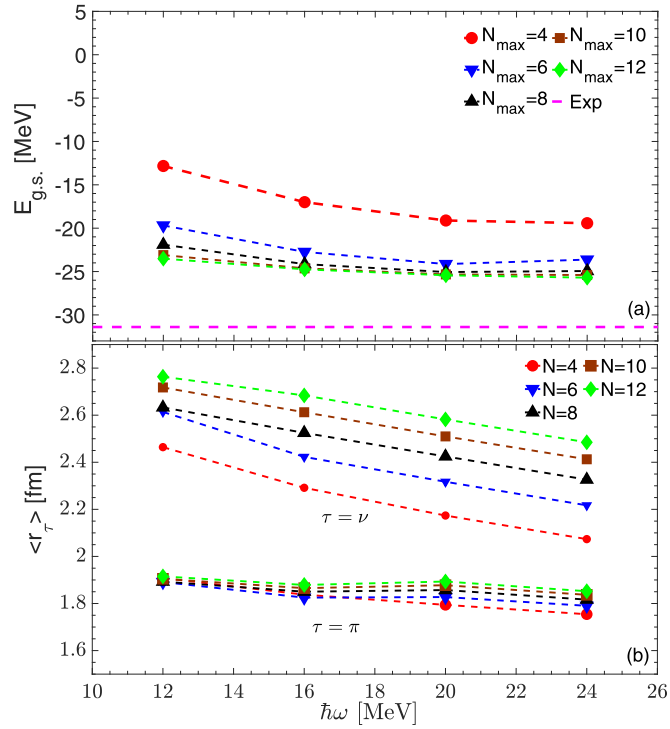

FIG. 1. Ground-state energy (a) and HF proton and neutron radii (b) versus the HO frequency for different dimensions $N_{\rm max}$. The dashed line indicates the experimental value [43].

It is not easy to find the reason of this discrepancy. It may be due partly to the more restricted HO configuration space we used, $N_{\rm max} = 12$ and $E_{3\,\rm max} = 12\hbar\omega$ compared to $N_{\rm max} = 14$ and $E_{3\,\rm max} = 16\hbar\omega$. Moreover, we have neglected the coupling between HF and three-phonon states (3p-3h) induced by the normal-ordered residual three-body force. Such a contribution was estimated to leading order within CC in Ref. [39], where V_S was derived, and, specifically for ^{8}He, in Ref. [28] using the same potential.

It is worth to point out that the energy is due mainly to the two-phonon correlations, $E_0^{\rm (corr)} = -20.1$ MeV. HF accounts only for $\sim$20%. Though contributing marginally to the energy, HF is by far the dominant component ($\sim$80%) of the ground-state wave function and yields realistic s.p. energies (Fig. 2) in qualitative agreement with those determined within the mentioned EDF approach [29].

It is also to be noted that the spurious contribution coming from the c.m. motion decreases as the dimensions $N_{\rm max}$ increase and eventually becomes negligible. In fact, it ranges from $\approx$800 keV for $N_{\rm max} = 4$ to $\approx$100 keV for $N_{\rm max} = 12$.

We make use of Eq. (13) to evaluate the neutron ($\tau = \nu$) and proton ($\tau = \pi$) radii $r_\tau = \sqrt{\langle r_\tau^2\rangle}$, where

$$\langle r_\tau^2\rangle = \frac{1}{N_\tau}\left(\langle\Psi_0|\sum_{i=1}^{N_\tau}(\vec{r}_\tau(i) - \vec{R}_{\rm c.m.})^2\,|\Psi_0\rangle\right). \tag{15}$$

We refer the nucleonic coordinates to the c.m. in order to minimize spurious contributions to the HF mean value, the only quantity which may be affected by the c.m. in our approach.

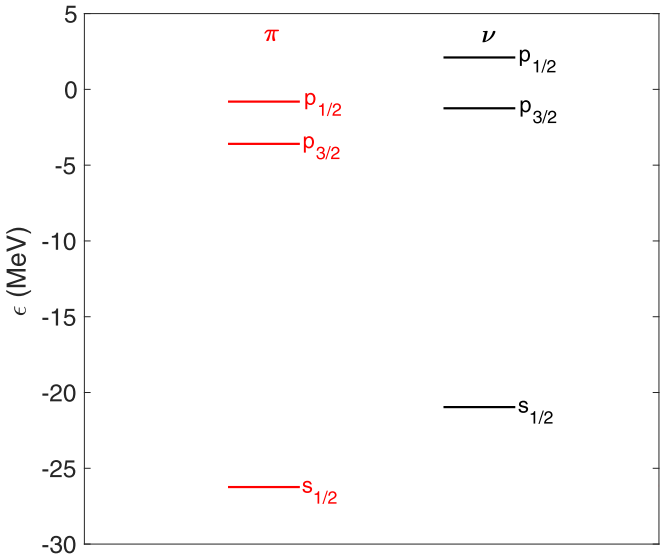

FIG. 2. HF proton and neutron single-particle energies.

We have also neglected the cross terms [$\propto \vec{r}_i \cdot \vec{r}_j (i \neq j)$] consistently with Refs. [44,45].

The neutron radius is extracted from the measured matter radius [18], and the proton one is derived from the experimental charge radius $r_{\rm ch}$ [20] through

$$\langle r_{\rm ch}^2 \rangle = \langle r_\pi^2 \rangle + R_p^2 + \frac{N}{Z} R_n^2 + \frac{3}{4m_p^2} + R_{\rm so}^2, \tag{16}$$

where $R_p = 0.8414(19)$ fm [46] is the proton charge radius, $R_n^2 = -0.106^{+0.007}_{-0.005}$ fm^2 [47] is the neutron charge square radius, the factor $3/(4m_p^2) = 0.033$ fm^2 is the Darwin-Foldy term, and $R_{\rm so}^2 = -0.143$ fm^2 is the spin-orbit correction taken from Ref. [28].

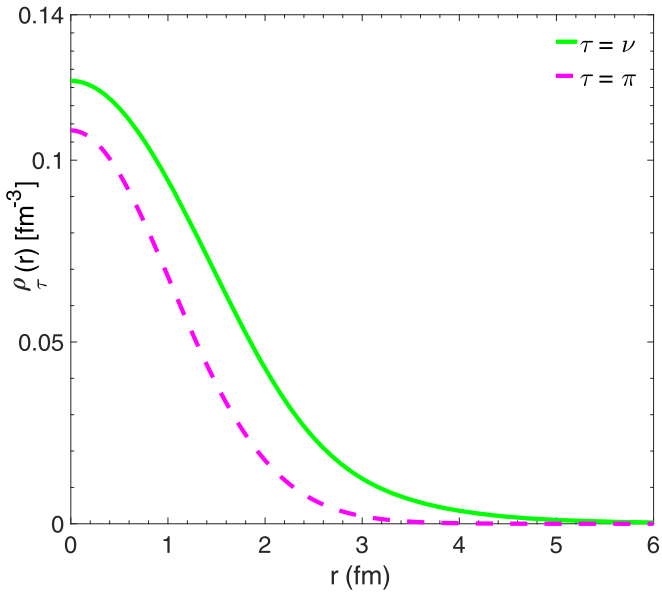

FIG. 3. HF neutron (ν) and proton (π) densities.

TABLE I. HF and EMPM charge, proton, and neutron radii $r_\tau = \sqrt{\langle r_\tau^2 \rangle}$ (in fm).

	$r_{\rm ch}$	r_π	r_ν	$r_\nu - r_\pi$
HF	1.95 (6)	1.88 (6)	2.7 (3)	0.8 (3)
EMPM	2.03 (6)	1.96 (6)	2.7 (3)	0.8 (3)
Exp	1.9559(165)	1.883(27)	2.71(8)	0.83(8)

The neutron over the proton excess, displayed in Fig. 3, determines the root-mean-square radii r_τ shown in Table I. All radii, as well as the neutron skin, are consistent with the corresponding empirical quantities. They are determined almost entirely by HF. As shown in Fig. 1(b), the convergence properties of the proton radius is fair with a maximum spreading of $\approx$0.06 fm. The convergence of the neutron radius versus frequency and space dimension is rather poor. The spreading amounts to $\approx$0.3 fm.

B. Spectrum

Figure 4 shows that the low-lying spectrum contains all levels that correspond to the experimental ones. It is to be pointed out that in this figure, as well as in the others, we use the excitation energies $\omega_\nu = E_\nu - E_{\rm HF}$ for n=1 (TD) and $\omega_\nu = \mathcal{E}_\nu - \mathcal{E}_0$ for n=2 and n=3. The eigenvalues $\mathcal{E}_\nu$ are defined in Eq. (10).

TD and EMPM yield the same number of levels in the low-lying sector of the spectrum. In fact, the corresponding eigenstates have a one-phonon dominance ($\gtrsim$80%). No two-phonon intruders occur. However, the multiphonon basis states play the important role of redistributing the levels and enhancing the separation between the lowest ones consistently with the experiments.

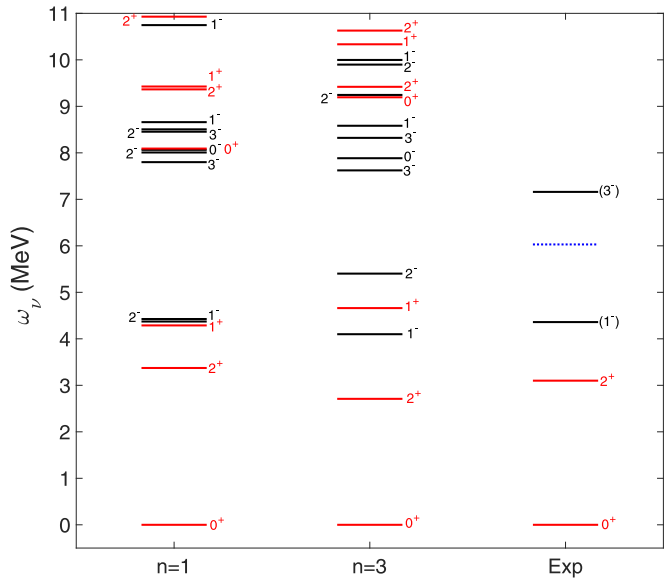

FIG. 4. TD and EMPM spectra. The experimental data are from Ref. [43].

C. Dipole response

We first compute the reduced strength

$$B_\nu(E1) = |\langle \Psi_\nu \parallel \mathcal{M}(E1) \parallel \Psi_0\rangle|^2 \tag{17}$$

of the electric dipole ($E1$) transition from the ground to the $\nu_{\rm th}$ states [Eq. (13)]

$$\langle \Psi_\nu \| \mathcal{M}(E1) \| \Psi_0\rangle = \sum_{\alpha_n \alpha_{n'}} \mathcal{C}^0_{\alpha_n} \mathcal{C}^\nu_{\alpha_{n'}} \langle \alpha_{n'} \| \mathcal{M}(E1) \| \alpha_n\rangle, \tag{18}$$

where

$$\mathcal{M}(E1,\mu) = e \sum_{k=1}^{A} \frac{1-\tau_3}{2} r_k Y_{1\mu}(\hat{r}_k). \tag{19}$$

We point out that the c.m. contribution is zero since our multiphonon wave functions are c.m. spurious free. Therefore, the present calculation may be also viewed as a test of the subtraction procedure operated within the EDF approach [29].

The $E1$ strength is used to evaluate the absorption cross section

$$\sigma = \int \sigma(\omega) d\omega = \frac{16\pi^3}{9} \frac{e^2}{\hbar c} m_1, \tag{20}$$

where m_1 is the first moment

$$m_1 = \int \omega \mathcal{R}(\omega) d\omega, \tag{21}$$

and

$$\mathcal{R}(\omega) = \frac{1}{e^2} \sum_\nu B_\nu(E1)\, \delta(\omega - \omega_\nu), \tag{22}$$

the response function. The δ function is replaced with a Lorentzian having a width $\Delta = 4$ MeV in the numerical implementation.

The energy weighted sum can be related to the Thomas-Reiche-Kuhn sum rule through

$$m_1^{(cl)} = \frac{\hbar^2}{2m} \frac{9}{4\pi} \frac{NZ}{A} (1+\kappa), \tag{23}$$

where κ is the enhancement factor coming from the exchange- and velocity-dependent terms of the Hamiltonian. Finally, we compute the moments ($r = 0, -1$)

$$m_r = \frac{1}{e^2} \sum_\nu \omega_\nu^r B_\nu(E1). \tag{24}$$

The inverse moment yields the polarizability

$$\alpha_D = \frac{8\pi}{9} e^2 m_{-1} = \frac{8\pi}{9} \sum_\nu \frac{1}{\omega_\nu} B_\nu(E1). \tag{25}$$

With respect to TD, the multiphonon coupling redistributes the $E1$-reduced strength among the low-lying levels and produces damping and fragmentation at higher energy (Fig. 5). The figure shows distinctly how the coupling to three phonons brings the peaks back to the region of the TD spectrum. They were shifted upward for $n = 2$ because of the depression of the ground-state energy induced by the strong HF to two-phonon coupling. Such a mechanism is a general feature pointed out in previous EMPM calculations [33,36,37] as well as in a recent different approach [48].

The profile of the resulting cross-section $\sigma(\omega)$ (Fig. 6) is qualitatively similar to the one obtained within the EDF approach [29]. However, the conclusions we draw about the nature of the spectrum are different. In fact, let us get a more complete characterization of the 1^- states by evaluating the reduced transition strengths of the isoscalar $E1$ operator

$$\mathcal{M}_{\rm IS}(E1) = e \sum_{k=1}^{A} r_k^3 Y_{1\mu}(\hat{r}_k). \tag{26}$$

As shown in Fig. 7, there is a clear distinction between the low- and the high-energy sectors. Wherease the high-energy transitions are purely isovector, the low-energy states, responsible for the first hump in the cross section, are excited by

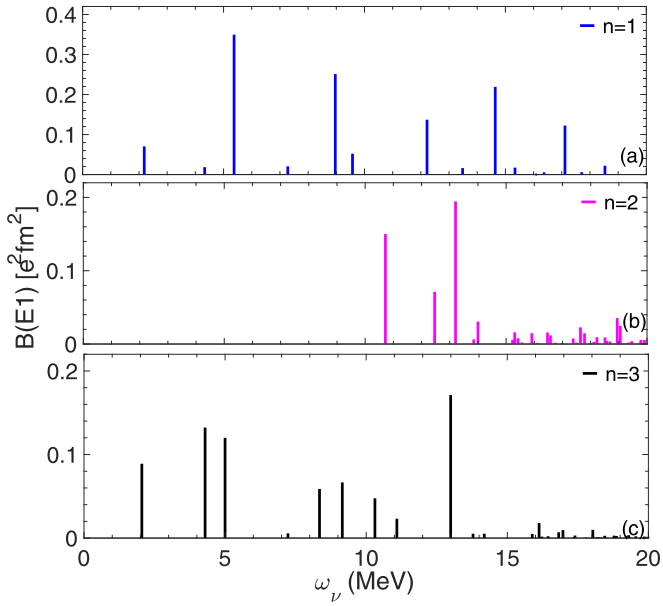

FIG. 5. $E1$ spectra computed within different multiphonon spaces. The different scales used in the panels are to be noted.

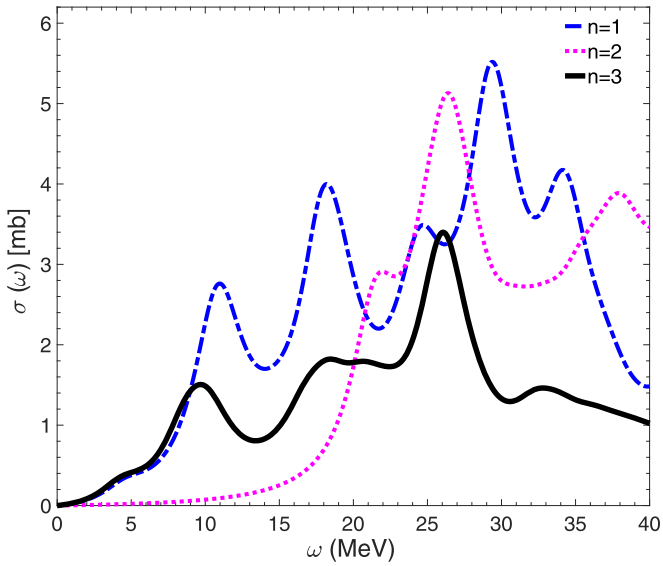

FIG. 6. $E1$ cross sections.

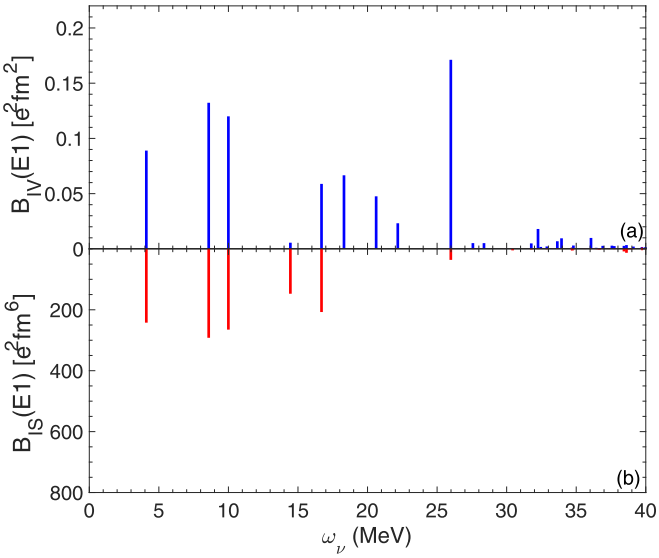

FIG. 7. Isovector versus isoscalar $E1$ transition strengths.

both isovector and isoscalar operators, a distinctive feature of a pigmy resonance.

For a better understanding we have computed the TD proton ($\tau = \pi$) and neutron ($\tau = \nu$) transition densities through

$$\langle \lambda \parallel \mathcal{M}_\tau(\lambda) \parallel 0 \rangle = \int dr\, r^2 r^\lambda \delta\rho^\tau_\lambda, \tag{27}$$

where

$$\delta\rho^\tau_\lambda = \sum_{\rm ph} c^\lambda_{\rm ph} \langle j_p l_p \parallel Y^\tau_\lambda(\hat{r}) \parallel j_h l_h \rangle R_{n_p l_p}(r) R_{n_h l_h}(r), \tag{28}$$

$R_{nl}(r)$ being the radial particle (p) and hole (h) wave functions.

As shown in Fig. 8, neutrons and protons oscillate in phase at low energy and in opposition of phase at high energy. It is interesting to observe the smooth transition from the low-lying to the high-energy regime. Thus, contrary to what suggested in Ref. [29], we do predict a low-energy soft mode. Unfortunately we cannot adopt the EMPM to evaluate the m_0 and m_1 momenta since we have extracted the eigenvectors up to $\omega_\nu \leqslant 60$ MeV. At higher energies, the spectrum includes many states with dominant three-phonon configurations, which couple to one- and two-phonon components. The description of these states would require an exact treatment of the three-phonon states. This goal, at the moment, is not within our reach. On the other hand, we checked that m_0 is strictly conserved in going from TD ($n = 1$) to the space including also the two-phonon basis. We verified that also m_1 is preserved if the energy shift of the ground state induced by the two-phonon coupling is ignored and the energies are referred to HF. This is what is done also in the extensions of both TD and RPA and was discussed in Ref. [38]. Thus, we expect the conservation of these quantities in the space including up to three phonons, if properly treated.

Therefore, we take TD as a term of comparison. We get $m_0 = 1.44$ fm^2 and $m_1 = 32.92$ MeV fm^2. The m_1 exceeds

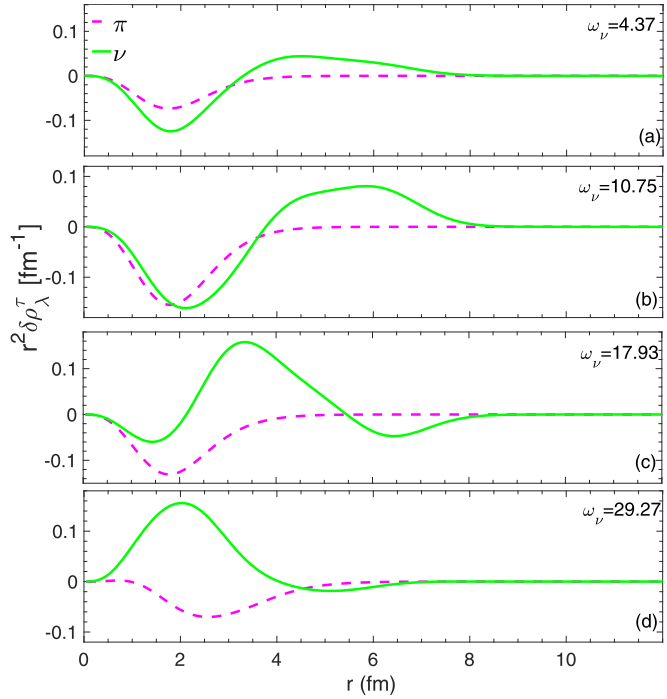

FIG. 8. Proton ($\tau = \pi$) and neutron ($\tau = \nu$) $\lambda = 1$ transition densities at different energies.

the energy weighted sum rule (EWSR) by a factor $1 + \kappa = 1.5$. The moment obtained within the EDF approach is fully consistent with the EWSR ($\kappa = 0$) [29]. CC [28], although using the same potential V_S adopted here, yields a larger enhancement ($1 + \kappa \sim 2$). This discrepancy is fictitious in our opinion. From comparing our Eq. (20) with the corresponding CC Eq. (20) [28], we obtain just $(m_1)_{CC} = \frac{4\pi}{9} m_1 \sim 1.4 m_1$. Apparently, the ratio between the two formulas is absorbed in the enhancement factor used in CC.

The inverse moment m_{-1} and, consequently, α_D are determined mainly by the low-energy transitions. Thus, even our truncated EMPM calculation yields a reliable estimate. As shown in Fig. 9, m_{-1} saturates at the value $m_{-1} = 0.074$ MeV^{-1} fm^2, yielding a polarizability $\alpha_D = 0.206$ fm^3. It came out to be $\sim$0.8 times the TD values, $m_{-1} = 0.090$ MeV^{-1} fm^2, $\alpha_D = 0.252$ fm^3. Both TD and EMPM estimates are roughly consistent with those obtained within the EDF [29] approach. They are appreciably smaller than the CC [28]. On the other hand, as for the first moment m_1, the discrepancy is to be attributed to the different definitions adopted in the two approaches.

IV. CONCLUDING REMARKS

We have seen that our multiphonon approach provides an exhaustive description of bulk and spectroscopic properties of the halo ^{8}He. It accounts only for 80% of the binding energy, which is instead reproduced in other CC calculations [28,39] using the same potential. The reason of this underestimation cannot be ascribed to the method, which was shown to be perfectly equivalent to an exact diagonalization of the Hamiltonian in the np-nh ($n = 0, 1, 2 \ldots$) configuration space

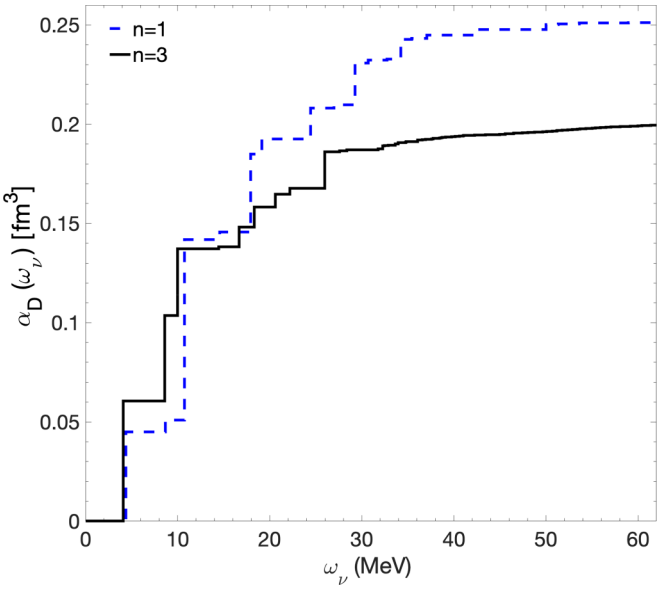

FIG. 9. The running sum determining the dipole polarizability α_D.

[38]. We can make only conjectures, such as the truncation of the space and/or the missing contribution coming from the residual normal-ordered three-body potential.

On the other hand, our calculation yields radii and neutron skin fairly close to the corresponding empirical quantities. The level scheme is consistent with the available experimental spectrum. This agreement is reached thanks to the coupling to the 3p-3h configurations incorporated into the three-phonon basis states.

This consistency could not be achieved if the spurious admixtures induced by the c.m. motion were not removed. This is a peculiarity of our method, which has a crucial impact on the nuclear response.

The global properties of the electric dipole response, namely dipole and inverse dipole moments, are consistent with the EDF results and with CC if we take for granted the different definitions adopted in Ref. [28]. The behavior of the cross section is qualitatively similar to the one exhibited by the EDF corresponding quantity. However, contrary to the conclusions drawn in that approach, our detailed analysis suggests two distinct collective motions, a low-energy soft mode and the standard giant resonance. This issue may be hopefully clarified by the incoming and/or other future experiments.

ACKNOWLEDGMENTS

We thank P. Navrátil for having provided the matrix elements of the NNLO$_{\rm sat}$ potentials. This work was cofunded by EU-FESR, PON Ricerca e Innovazione 2014-2020-DM 1062/2021. It was also partly supported by the Czech Science Foundation (Czech Republic), Grant No. P203-23-06439S and by the Charles University Research Center Grant No. UNCE/SCI/013. Computational resources were provided by the CESNET LM2015042 and the CERIT Scientific Cloud Grant No. LM2015085, under the program "Projects of Large Research, Development, and Innovations Infrastructures."

[1] K. Blaum, J. Dilling, and W. Nörtershäuser, Phys. Scr., T **152**, 014017 (2013).
[2] I. Tanihata, H. Hamagaki, O. Hashimoto, Y. Shida, N. Yoshikawa, K. Sugimoto, O. Yamakawa, T. Kobayashi, and N. Takahashi, Phys. Rev. Lett. **55**, 2676 (1985).
[3] I. Tanihata, T. Kobayashi, O. Yamakawa, S. Shimoura, K. Ekuni, K. Sugimoto, N. Takahashi, T. Shimoda, and H. Sato, Phys. Lett. B **206**, 592 (1988).
[4] M. Zhukov, B. Danilin, D. Fedorov, J. Bang, I. Thompson, and J. Vaagen, Phys. Rep. **231**, 151 (1993).
[5] G. Hagen, D. Dean, M. Hjorth-Jensen, and T. Papenbrock, Phys. Lett. B **656**, 169 (2007).
[6] S. Bacca, N. Barnea, W. Leidemann, and G. Orlandini, Phys. Rev. Lett. **102**, 162501 (2009).
[7] S. Bacca, N. Barnea, and A. Schwenk, Phys. Rev. C **86**, 034321 (2012).
[8] E. Caurier and P. Navrátil, Phys. Rev. C **73**, 021302(R) (2006).
[9] P. Maris, J. P. Vary, and P. Navrátil, Phys. Rev. C **87**, 014327 (2013).
[10] C. Romero-Redondo, S. Quaglioni, P. Navrátil, and G. Hupin, Phys. Rev. Lett. **117**, 222501 (2016).
[11] M. A. Caprio, P. Maris, and J. P. Vary, Phys. Rev. C **90**, 034305 (2014).
[12] Z. H. Sun, T. D. Morris, G. Hagen, G. R. Jansen, and T. Papenbrock, Phys. Rev. C **98**, 054320 (2018).
[13] R. B. Wiringa, S. C. Pieper, J. Carlson, and V. R. Pandharipande, Phys. Rev. C **62**, 014001 (2000).
[14] G. Papadimitriou, A. T. Kruppa, N. Michel, W. Nazarewicz, M. Płoszajczak, and J. Rotureau, Phys. Rev. C **84**, 051304(R) (2011).
[15] Y. Jaganathen, R. M. Id Betan, N. Michel, W. Nazarewicz, and M. Płoszajczak, Phys. Rev. C **96**, 054316 (2017).
[16] T. Myo, M. Odsuren, and K. Katō, Phys. Rev. C **104**, 044306 (2021).
[17] T. Myo and K. Katō, Phys. Rev. C **107**, 034305 (2023).
[18] X. Liu, P. Egelhof, O. Kiselev, and M. Mutterer, Phys. Rev. C **104**, 034315 (2021).
[19] M. Brodeur, T. Brunner, C. Champagne, S. Ettenauer, M. J. Smith, A. Lapierre, R. Ringle, V. L. Ryjkov, S. Bacca, P. Delheij *et al.*, Phys. Rev. Lett. **108**, 052504 (2012).
[20] P. Mueller, I. A. Sulai, A. C. C. Villari, J. A. Alcántara-Núñez, R. Alves-Condé, K. Bailey, G. W. F. Drake, M. Dubois, C. Eléon, G. Gaubert *et al.*, Phys. Rev. Lett. **99**, 252501 (2007).
[21] J. J. Krauth, K. Schuhmann, M. A. Ahmed, F. D. Amaro, P. Amaro, F. Biraben, T.-L. Chen, D. S. Covita, A. J. Dax, M. Diepold *et al.*, Nature (London) **589**, 527 (2021).
[22] G. Alkhazov, A. Dobrovolsky, P. Egelhof, H. Geissel, H. Irnich, A. Khanzadeev, G. Korolev, A. Lobodenko, G. Münzenberg, M. Mutterer *et al.*, Nucl. Phys. **A712**, 269 (2002).

[23] M. Golovkov, L. Grigorenko, G. Ter-Akopian, A. Fomichev, Y. Oganessian, V. Gorshkov, S. Krupko, A. Rodin, S. Sidorchuk, R. Slepnev *et al.*, Phys. Lett. B **672**, 22 (2009).
[24] Y. Iwata, K. Ieki, A. Galonsky, J. J. Kruse, J. Wang, R. H. White-Stevens, E. Tryggestad, P. D. Zecher, F. Deák, A. Horváth *et al.*, Phys. Rev. C **62**, 064311 (2000).
[25] K. Markenroth, M. Meister, B. Eberlein, D. Aleksandrov, T. Aumann, L. Axelsson, T. Baumann, M. Borge, L. Chulkov, W. Dostal *et al.*, Nucl. Phys. **A679**, 462 (2001).
[26] M. Meister, K. Markenroth, D. Aleksandrov, T. Aumann, T. Baumann, M. Borge, L. Chulkov, D. Cortina-Gil, B. Eberlein, T. Elze *et al.*, Nucl. Phys. A **700**, 3 (2002).
[27] M. Holl, R. Kanungo, Z. Sun, G. Hagen, J. Lay, A. Moro, P. Navrátil, T. Papenbrock, M. Alcorta, D. Connolly *et al.*, Phys. Lett. B **822**, 136710 (2021).
[28] F. Bonaiti, S. Bacca, and G. Hagen, Phys. Rev. C **105**, 034313 (2022).
[29] J. Piekarewicz, Phys. Rev. C **105**, 044310 (2022).
[30] T. Myo and K. Katō, Phys. Rev. C **106**, L021302 (2022).
[31] F. Andreozzi, F. Knapp, N. Lo Iudice, A. Porrino, and J. Kvasil, Phys. Rev. C **75**, 044312 (2007).
[32] F. Andreozzi, F. Knapp, N. Lo Iudice, A. Porrino, and J. Kvasil, Phys. Rev. C **78**, 054308 (2008).
[33] D. Bianco, F. Knapp, N. Lo Iudice, F. Andreozzi, and A. Porrino, Phys. Rev. C **85**, 014313 (2012).
[34] G. De Gregorio, F. Knapp, N. Lo Iudice, and P. Veselý, Phys. Rev. C **93**, 044314 (2016).
[35] D. Bianco, F. Knapp, N. Lo Iudice, P. Veselý, F. Andreozzi, G. De Gregorio, and A. Porrino, J. Phys. G: Nucl. Part. Phys. **41**, 025109 (2014).
[36] G. De Gregorio, F. Knapp, N. Lo Iudice, and P. Veselý, Phys. Lett. B **821**, 136636 (2021).
[37] G. De Gregorio, F. Knapp, N. Lo Iudice, and P. Veselý, Phys. Rev. C **105**, 024326 (2022).
[38] F. Knapp, P. Papakonstantinou, P. Veselý, G. De Gregorio, J. Herko, and N. Lo Iudice, Phys. Rev. C **107**, 014305 (2023).
[39] A. Ekström, G. R. Jansen, K. A. Wendt, G. Hagen, T. Papenbrock, B. D. Carlsson, C. Forssén, M. Hjorth-Jensen, P. Navrátil, and W. Nazarewicz, Phys. Rev. C **91**, 051301(R) (2015).
[40] G. Hagen, T. Papenbrock, D. J. Dean, A. Schwenk, A. Nogga, M. Włoch, and P. Piecuch, Phys. Rev. C **76**, 034302 (2007).
[41] R. Roth, S. Binder, K. Vobig, A. Calci, J. Langhammer, and P. Navrátil, Phys. Rev. Lett. **109**, 052501 (2012).
[42] G. Hagen, T. Papenbrock, A. Ekström, K. A. Wendt, G. Baardsen, S. Gandolfi, M. Hjorth-Jensen, and C. J. Horowitz, Phys. Rev. C **89**, 014319 (2014).
[43] Data extracted using the NNDC On-line Data Service from the ENSDF database, https://www.nndc.bnl.gov/ensdf.
[44] B. S. Hu, F. R. Xu, Z. H. Sun, J. P. Vary, and T. Li, Phys. Rev. C **94**, 014303 (2016).
[45] G. De Gregorio, J. Herko, F. Knapp, N. Lo Iudice, and P. Veselý, Phys. Rev. C **95**, 024306 (2017).
[46] E. Tiesinga, P. J. Mohr, D. B. Newell, and B. N. Taylor, Rev. Mod. Phys. **93**, 025010 (2021).
[47] A. A. Filin, V. Baru, E. Epelbaum, H. Krebs, D. Möller, and P. Reinert, Phys. Rev. Lett. **124**, 082501 (2020).
[48] Y. Beaujeault-Taudière, M. Frosini, J.-P. Ebran, T. Duguet, R. Roth, and V. Somà, Phys. Rev. C **107**, L021302 (2023).